Journal of CO2 Utilization 53 (2021) 101721

Contents lists available at ScienceDirect

Journal of CO2 Utilization

journal homepage: www.elsevier.com/locate/jcou

Performance of supported metal catalysts in the dimethyl carbonate production by direct synthesis using CO_2 and methanol

Douglas José Faria [a], Leonardo Moreira dos Santos [b], Franciele Longaray Bernard [b], Ingrid Selbacch Pinto [b], Ivan Pacheco Romero [c], Vitaly V. Chaban [d], Sandra Einloft [a,b,*]

[a] Post-Graduation Program in Materials Engineering and Technology, Pontifical Catholic University of Rio Grande do Sul – PUCRS, Brazil
[b] School of Technology, Pontifical Catholic University of Rio Grande do Sul PUCRS, Brazil
[c] CENPES/Petrobras, Brazil
[d] P.E.S., Vasilievsky Island, Saint Petersburg, Russian Federation

ARTICLE INFO

Keywords:
Dimethyl carbonate
CO_2
Methanol
Catalysts
Synthesis

ABSTRACT

CO_2 chemical transformation is an exciting way to reduce CO_2 concentration in the atmosphere. The use of CO_2 to produce dimethyl carbonate (DMC), a linear, biodegradable, low toxicity carbonate via direct synthesis, is one of the most promising routes from the environmental point of view. However, DMC direct synthesis presents obstacles such as unfavorable thermodynamics and catalytic deactivation due to the water produced as a by-product. Therefore, the development and optimization of a catalytic system that can overcome these obstacles are crucial. This study investigated the catalytic activity of iron nitrate (AC-Fe), copper nitrate (AC-Cu), magnesium nitrate (AC-Mg), and nickel nitrate (AC-Ni) impregnated in activated carbon for DMC direct synthesis. Catalysts were synthesized by the impregnation method and characterized by several techniques. Simulation results evidenced the major reaction steps and simplified models of a complex involving metallic catalysts and reactants. The optimization of the catalyst amount, pressure, temperature, and recyclability of the best catalyst under optimized conditions and in the presence of different dehydrating agents was also performed. Results showed that the AC-Fe catalyst is the most efficient in the DMC direct synthesis, with a yield of 23.5 % and a selectivity of 100 % (80 °C, 40 bar, and 24 h). Reaction optimization (120 °C, 40 bar, and 24 h) using (AC-Fe) as catalyst resulted in a DMC yield of approximately 30 %. The catalytic systems recycling proved that using the dehydrating agent right combination (molecular sieve) and catalyst (AC-Fe) can maintain selectivity at 100 %, slightly decreasing yield.

1. Introduction

The application of carbon dioxide as a raw material in the chemical industries is vital from an environmental perspective. However, industrial processes using CO_2 as a starting material are few, mainly due to the large amount of energy required for its transformation [1]. Thus, some of the methodologies for transposing the CO_2 transformation into useful chemical products consist of using high-energy starting materials, such as hydrogen, unsaturated compounds, low-carbon, and organometallic rings. Also, choosing low-energy oxidized synthetic targets, such as organic carbonates, represents a crucial strategy [2,3]. Besides, in reactions to synthesize DMC, it is necessary to use a catalyst, which can be homogeneous, heterogeneous, or enzymatic. Promoting agents, such as iodomethane, can also be used [4,5].

Carbonates produced from CO_2 chemical transformation must be mentioned because they can selectively and efficiently replace hazardous reagents in organic processes [6,7]. Organic carbonates can be divided into two groups: linear carbonates (DMC and diethyl carbonate (DEC)); and cyclic carbonates: ethylene carbonate (CE), propylene carbonate (CP), butylene carbonate (CB), and glycerol carbonate (CG) [6–10]. Fig. 1 shows the structures of the main carbonates.

DMC is an essential chemical intermediate of easy degradability, high polarity, low viscosity, and toxicity used in various applications. For example, DMC is a raw material in polycarbonate synthesis, a widely used polymer in construction, automobiles, medical devices, and electrolyte solvent for lithium batteries due to its high dielectric constant and an environmentally friendly reagent for methylation and carbonylation [4,10–13].

* Corresponding author at: Post-Graduation Program in Materials Engineering and Technology, Pontifical Catholic University of Rio Grande do Sul – PUCRS, Brazil.
E-mail address: einloft@pucrs.br (S. Einloft).

https://doi.org/10.1016/j.jcou.2021.101721
Received 3 July 2021; Received in revised form 8 September 2021; Accepted 14 September 2021
Available online 22 September 2021

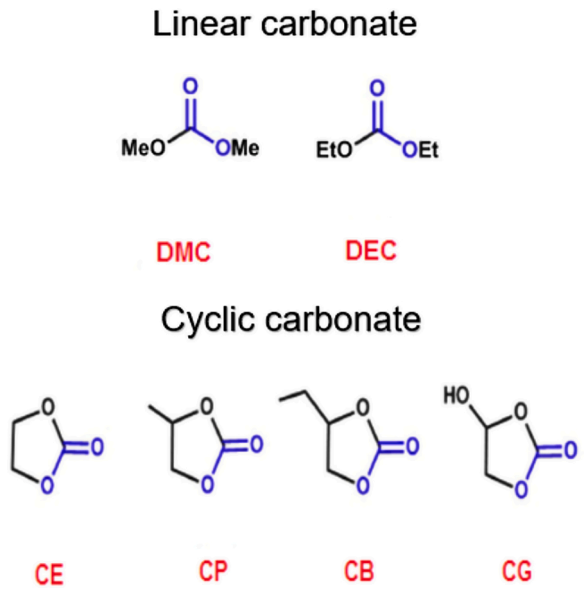

Fig. 1. Main linear and cyclic organic carbonates [9].

DMC can be synthesized by several routes, such as phosgene, transesterification, urea alcoholization, oxidative methanol carbonylation, and direct synthesis from methanol and CO_2 [11]. Phosgenation, oxidative carbonylation of methanol (oxycarbonylation) in a liquid phase, and transesterification processes reached industrialization. However, due to the high toxicity of the raw material (phosgene), the phosgenation route was discontinued. In contrast, DMC industrial production by oxycarbonylation and transesterification routes is a mature technology. The use of these routes in DMC production has some drawbacks, including the high toxicity of reagents and equipment corrosion [11,12,14].

To overcome these disadvantages, the direct synthesis of DMC is extensively studied to promote an increase in DMC yield and, at the same time, use non-toxic reagents that do not enable corrosion of tanks and other equipment [6,7,12,15–25]. Fig. 2 shows the scheme of the direct synthesis of DMC.

Homogeneous catalysts can produce DMC through direct synthesis. Among them are thallium (I) hydroxide, tin (IV) tetralkoxides, dialkytin dialkoxides, bases, C/N-chelated organotin (IV) trifluoromethane sulfonates [4,12,26–34]. However, the use of homogeneous catalysts presents, as the central challenge, catalyst separation from the reaction medium. Therefore, heterogeneous catalysts, such as CeO_2 and ZrO_2 [7, 15], $Ce_{0.5}Zr_{0.5}O_2$ [31], $Ce_{0.4}Zr_{0.6}O_2$ [20], and Cu-CeO_2 can overcome this drawback [35].

In addition to using several kinds of catalysts, one can use catalytic supports, such as silica, activated carbon, alumina, among others [36]. The use of supports should be explored to increase DMC production yield due to the structural, chemical, and thermal properties that help catalytic activity [37]. One of the most studied supports is activated carbon. Oxygen-containing sites in the carbon's structure facilitate the adsorption of metal ions (catalysts). Besides, hydroxyls kept on inorganic supports tend to destabilize more easily impregnated catalysts, whose disruption does not occur with the use of activated carbon [36, 38]. Several studies have analyzed the use of activated carbon to support impregnation of the metal ions and concluded that the catalytic activity is increased by support porosity, allowing the reuse of supported

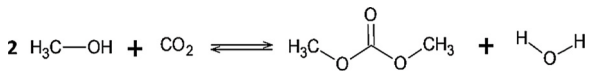

Fig. 2. Direct synthesis of DMC [4].

catalysts [39–41]. Thus, the support efficiency can be rated as follows: activated carbon > alumina > zeolite > silica [37].

Herein, we report the impregnation of different metals in activated carbon. The obtained samples were characterized and evaluated as catalysts in the DMC direct synthesis. The results from the simulation evidenced the main reaction steps providing simplified models for the metals-reactants complexes. The use of molecular sieves as dehydrating agents and iodomethane (CH_3I) as a promoter was also tested. The recycling of the best-supported catalyst was evaluated in the DMP synthesis using different dehydrating agents and sieves.

2. Methodology

2.1. Materials

Methanol (> 99.9 % - EMSURE®), iodomethane (> 99.5 % - ALDRICH), diethyl ether (> 99.9 % - ALDRICH), dimethyl carbonate - DMC (> 99.5 % - ALDRICH), activated carbon (CarboActiv G Plus Brascarbo- 325mesh), iron (III) nitrate nonahydrate (> 98.5 % - ALDRICH), copper (II) nitrate trihydrate (> 99.0 % - ALDRICH), nickel (II) nitrate hexahydrate (> 99.5 % - ALDRICH), magnesium nitrate hexahydrate (> 99.9 % - ALDRICH), pearl-shaped molecular sieves (3A - ALDRICH), 2,2-dimethoxypropane (98 % - ALDRICH) and CO_2 (99.8 % - White Martins).

2.2. Synthesis of metallic catalysts by the impregnation method in substrates

The catalysts were synthesized using the evaporation impregnation method [42]. This method consists of preparing a solution containing 10 g of the support material (activated carbon) and 1.7 g of different metal nitrates (iron, copper, magnesium, and nickel) in 250 ml of distilled water. Afterward, the solution is kept under constant agitation and at a temperature of 60 °C for 24 h; it is placed in an oven at 100 °C overnight and, finally, calcined at 600 °C for 3 h.

2.3. Characterization of supported metal ions

2.3.1. Thermogravimetric analysis (TGA)

Thermogravimetric analysis (TGA) was performed using a TA Instruments model Q600 equipment, ranging from room temperature to 1000 °C, with a heating rate of 20 °C/min under a synthetic air atmosphere. The calculation to determine the actual impregnation (%) of the metals in the activated carbon sample was carried out according to Eq. 1, where the difference among the metal impregnated carbon (ACX) sample weight and the weight of the pure carbon (AC) sample in the temperature range of 25–800 °C gives the percentage of impregnation [43].

$$\% = (wt\%\ ACX\ 25 - 800\ ^{\circ}C) - (wt\%\ AC\ 25 - 800^{\circ}C) \quad (1)$$

2.3.2. Scanning electron microscopy with field emission (SEM-FEG)

Analysis of Scanning Electron Microscopy with Field Emission (SEM-FEG) was performed using FEI Inspect F50 equipment in the mode of secondary electrons (SE). The films were placed in a stub and covered with a gold foil.

2.3.3. BET

The specific surface area was calculated based on the Brunauer-Emmet-Teller (BET) method. The pore size and the pore volume were determined by the Barret-Joyner-Halenda method. Before all analysis, samples were degassed at 150 °C for at least 3 h.

2.3.4. FTIR-UATR

The chemical structures of supported catalysts and activated carbon were assessed by infrared spectroscopy technique using a Perkin - Elmer

100 Spectrum at wavenumber range 4000–650 cm^{-1} with accessory UATR (universal attenuated total reflectance). All samples were analyzed in the form of powder.

2.3.5. XRD

The samples were placed in the sample holder of the Shimadzu model XRD 7000 (X-Ray Powder Diffraction) equipment and analyzed between 2 and 70 degrees (the region where the most intense peaks can appear). Copper k alpha radiation was used for analysis, and parallel geometry support was used for the surface analysis.

2.4. DMC synthesis

A 120 mL reactor (made of a titanium alloy) with constant magnetic stirring was used to perform the experiments. The temperature was controlled using a thermocouple connected to a temperature controller and kept steady using a resistive thermal band in both reactors. The reactor was equipped with metallic compartment support in the gas phase filled with molecular sieves [4]. For a typical reaction, 213 mmol of methanol, 0.7 g metal impregnated activated carbon, 20 mmol of CH_3I, 2.0 g of molecular sieves, and 40 bar of CO_2 were used. The reactor was pressurized with CO_2 at 40 bar and heated at 80 °C. At the end of the reaction, the reactor was cooled to room temperature and slowly depressurized.

The best-performance catalyst was used to optimize the temperature (80, 105, and 130 °C) and pressure (40, 45, and 50 bar) parameters in direct DMC synthesis. Finally, an analysis of 4 recycles was performed using the best catalyst supported on the activated carbon. After each reaction, the catalyst was washed several times in methanol and dried in an oven overnight. Catalyst reuse evaluation was performed using three different systems, namely A: 3A molecular sieve (dehydrating agent); B: DMP (dehydrating agent); C: molecular sieve (gas phase) combined with DMP (liquid phase), as described in previous work [4]. The reaction conditions were as follows: pressure: 40 bar; temperature: 120 °C; time: 24 h; 0.7 g of AC-Fe; 2.0 g molecular sieve; 10 mmol of DMP; 213 mmol of methanol; 20 mmol of CH_3I.

All reaction tests were performed in triplicate and analyzed by gas chromatography (GC) to determine yield, conversion, and selectivity [4]. The equipment used was the Gas Chromatograph *Shimadzu* GC-2014 with SH-Rtx-5 column and the programming of 31 °C for 0.5 min, rate of 10 °C / min to 50 °C for 1 min, rate of 20 °C / min to 100 °C for 2 min and rate of 50 °C / min to 220 °C for 2 min. The samples were diluted with a concentration of 4 % (v/v) in ethyl ether and injected into the GC to determine the DMC peak area (2.4–2.7 minutes). The calculations performed to determine conversion, selectivity, and yield were achieved according to Faria et al. [4].

Methanol conversion was calculated using Eq. 2.

$$Methanol\ conversion\ (\%) = ((Methanol\ reacted)/(\text{Methanol total})) * 100 \quad (2)$$

DMC selectivity was obtained by Eq. 3.

$$DMC\ selectivity\ (\%) = ((DMC)/(\text{DMC} + (\text{by} - \text{products}))) * 100 \quad (3)$$

DMC yield was determined using Eq. 4.

$$DMC\ yield\ (\%) = ((Methanol\ conversion\ (\%)) * (DMC\ selectivity(\%)))/100 \quad (4)$$

2.5. Statistical analysis

Minitab 18 Statistical Software-ANOVA was used to do statistical analysis to assess the standard deviation of tests performed in triplicate and analyze the Tukey test with 95 % reliability. Equal letters show statistical equivalence of the sample averages. Also, temperature and pressure parameters were optimized by analyzing the surface and contour graph.

2.6. Simulation methodology

Electronic-structure calculations and potential energy minimum search for multiple molecular structures were conducted using the GAMESS-US (2014) package of programs [44], Atomic Simulation Environment Toolkit (ASE) [45], Gabedit 2.8 [46], Visual Molecular Dynamics (VMD 1.9.1) [47], Avogadro [48], and in-home programs [49–51]. Molecular geometries corresponding to local-minimum structures (only positive vibrational frequencies) were subject to the calculation of thermochemical properties at different conditions.

The electronic structure of the simulated species was optimized by the hybrid density functional theory (M11 functional) [52] that includes dispersion interactions [53] and provides a generally decent quality of results in the case of organic moieties. The MIDI split-valence basis set [54] was used to construct molecular wave functions for every reactant and product. The electronic wave function convergence criterion was set to 1×10^{-3} kJ mol^{-1}. The steepest descent geometry optimization criterion was set to 0.5 kJ mol^{-1} for potential energy surface investigation and to 0.05 kJ mol^{-1} to derive thermochemical parameters. Frequency analysis was performed for optimized molecular structures, and the absence of negative frequencies in the profile was assured.

The Gibbs free energy of the reaction was calculated as a difference of the total Gibbs free energy of the products and the total Gibbs free energy of the reactants.

3. Results

3.1. Metal impregnated support characterization

3.1.1. TGA

Fig. 3 presents TGA analysis. All samples showed two stages of mass loss. In the first stage, moisture evaporation occurs (temperatures below 150 °C) [55–57], and AC presented the most significant loss of mass (18 %), followed by AC-Fe (14 %), AC-Ni (12 %) and, AC-Cu and AC-Mg (10 %). In the second degradation stage, the sample AC started the degradation at T = 420 °C, but the other impregnated metal-containing samples began the second degradation stage near T = 400 °C, which may be related to the loss of components from the lignin present in the coal [58]. The bare activated carbon (AC) sample showed a total mass loss of approximately 35.51 % due to structural decomposition. Samples mass loss were as follows: AC-Fe 17.13 %, AC-Cu (22.10 %), AC-Mg (27.34 %), and AC-Ni (29.48 %). Therefore, metals impregnation in the activated carbon is following the order: AC-Fe (18.38 ± 1.2 %)> AC-Cu (13.41 ± 0.7 %)>AC-Mg (8.17 ± 1.1 %)>AC-Ni (6.03 ± 0.9 %) in close agreement with ICP-OS analysis (see Table S1).

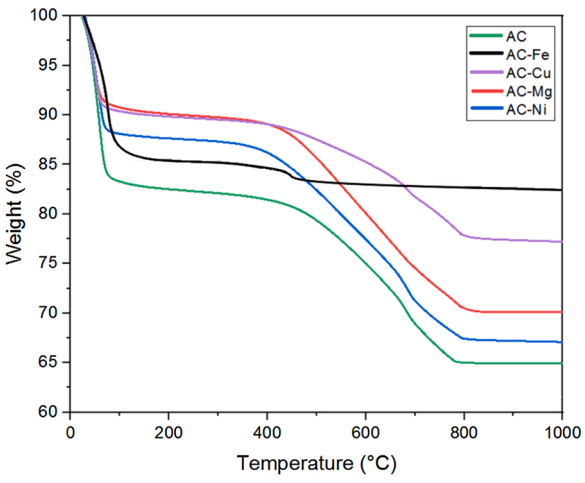

Fig. 3. TGA analysis of samples containing pure support and metals impregnated with activated carbon.

3.1.2. SEM-FEG

Different metal nitrates were impregnated in the activated carbon sample to evaluate their anchoring capacity with the support surface. Fig. 4 shows the SEM-FEG images of activated carbon (AC) and AC impregnated with different metals.

The micrographs of pure AC showed a surface with pores (mesopores/macropores/micropores). Such regions are essential because they serve to anchor metals on the support surface [59]. Activated carbon can be considered a very efficient support due to porous channels in its structure, facilitating metal impregnation [60]. Yet, dispersed and agglomerated particles in the activated carbon structure were observed in all samples. However, the anchoring of metals tends to occur more efficiently in the pores of the support structure, avoiding the anchored metal being leached as the catalyst is reused. EDS analysis for all samples is presented in Fig. S1 [61,62].

Metal insertion in the activated carbon porous cavities could cause changes in its structure [63]. One noticed particle agglomerates from the added metals in the impregnated activated carbon samples, indicating that the impregnation occurred satisfactorily [64–67]. The literature describes AC as a support with a relatively high surface area. Pore presence in AC is responsible for this morphological and structural characteristic facilitating CO_2 diffusion through the structure, benefiting its use when applied in catalysis [64,67,68].

3.1.3. BET

The specific surface area, pore-volume, and pore radius analysis are essential to determine the ability of the materials to impregnate the metal ions used as catalysts in the DMC direct synthesis [69,86]. Table 1 shows the specific surface area, pore-volume, and pore radius of synthesized samples analyzed by BET (Brunauer, Emmett, and Teller).

Activated carbon (AC) has a specific surface area value of 985 m^2 /g, a pore volume of 0.58 cm^3 /g, and an average pore radius of 1.5 nm. Yet, the N_2 adsorption-desorption isotherm (Fig. S2) is a type IV isotherm and type H4 hysteresis following Teng et al. [70]. The narrow hysteresis curve corresponds to the moderate presence of micropores in the material structure and a more important number of mesopores [71]. For all samples, metal impregnation promoted the increasing or maintenance of the pore radius, except for the case of copper impregnation, where we noticed an increase in the pore radius caused by the support structure disruption during impregnation [73,74]. A decrease in the AC-specific surface area and pore volume is expected due to metals impregnation in the micropores and deposition in the mesopores, causing channel blockage that decreases the pore volume. This behavior agrees with SEM-FEG results, indicating metal impregnation in porous channels and deposition on the support surface [39,60,72].

Table 1
Specific surface area, volume, and radius of pores of AC and impregnated iron nitrate (AC-Fe), copper nitrate (AC-Cu), magnesium nitrate (AC-Mg), and nickel nitrate (AC-Ni) samples.

Sample	BET (m^2/g)	Pore volume (cm^3/g)	Average pore radius (nm)
AC	985	0.58	1.5
AC-Fe$(NO_3)_3$	620	0.48	1.6
AC-Cu$(NO_3)_2$	177	0.22	2.5
AC-Mg$(NO_3)_2$	797	0.57	1.5
AC-Ni$(NO_3)_2$	569	0.42	1.5

3.1.4. FTIR

Fig. 5 presents FTIR spectra for the pure AC and AC-impregnated metal samples.

All samples showed bands around 3500 cm^{-1} attributed to OH (hydroxyl) groups. The AC sample showed a band at 900 - 1200 cm^{-1}, attributed to silicon present in the activated carbon structure (Fig. S1) related to two types of bonds (Si–OH and C–O). The band at approximately 3333 cm^{-1} for activated carbon indicates –OH bonds, and small bands at 1582 cm^{-1} and 1192 cm^{-1} C=C and C–O bonds, respectively [63,75–77].

For AC support impregnated with iron nitrate, bands close to 1550 cm^{-1} and 1400 cm^{-1} can indicate the presence of iron hydroxide particles, FeO(OH). Bands in the range of 701–709 cm^{-1} indicate hematite (Fe_2O_3) formation due to the support structure-metal interaction. Bands at 1000–1200 cm^{-1} show CO-type bonds present in the activated carbon support [78,79]. For AC-Cu, bands between 2100–2200 cm^{-1} can indicate C–H, and small bands close to 3000 cm^{-1} refer to the Cu-N bond [80]. A band around 1400 cm^{-1} is attributed to the metal (copper) attached to the hydroxyl group [81,87].

In the case of magnesium nitrate, the metal is in its oxidized form. A small absorption band around 1635 cm^{-1} refers to the Mg-NO_2 bond, vibrations of the carbonate groups on the surface were identified at 1384 cm^{-1}, and bands referring to MgO at 825 cm^{-1} [82,83]. For the composite AC-Mg, the –OH and –CH bonds are seen at 3427 cm^{-1} and 2921 cm^{-1}, respectively [84]. Vibration bands from carbonate groups of $MgCO_3$ appear at 1466, 1384, and 1124 cm^{-1} [84,85]. The band of metal in the oxidized form appears in the range of 900–400 cm^{-1} [85,

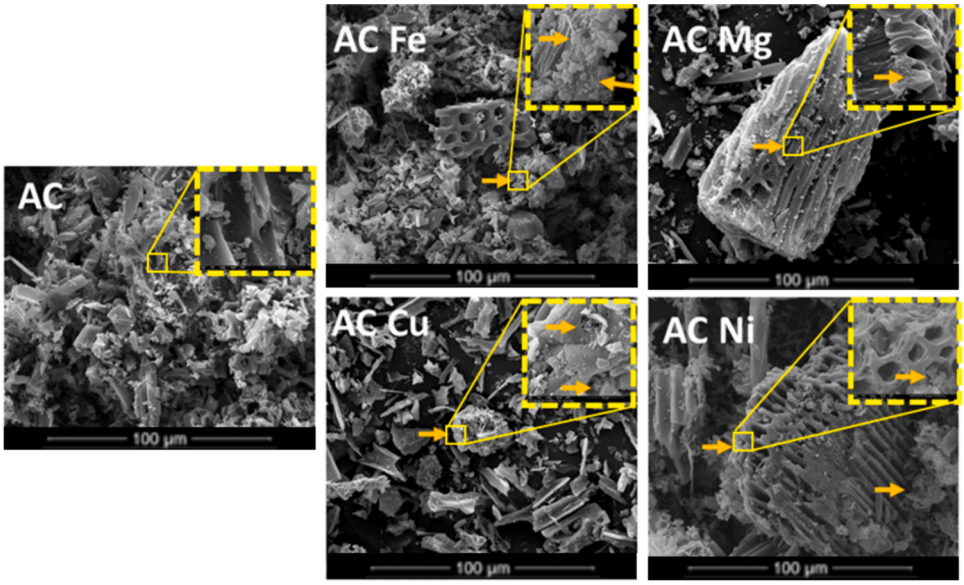

Fig. 4. MEV-FEG image of samples AC and AC-Fe, AC-Cu, AC-Mg, AC-Ni (augmentation 1000x and insert 10000x).

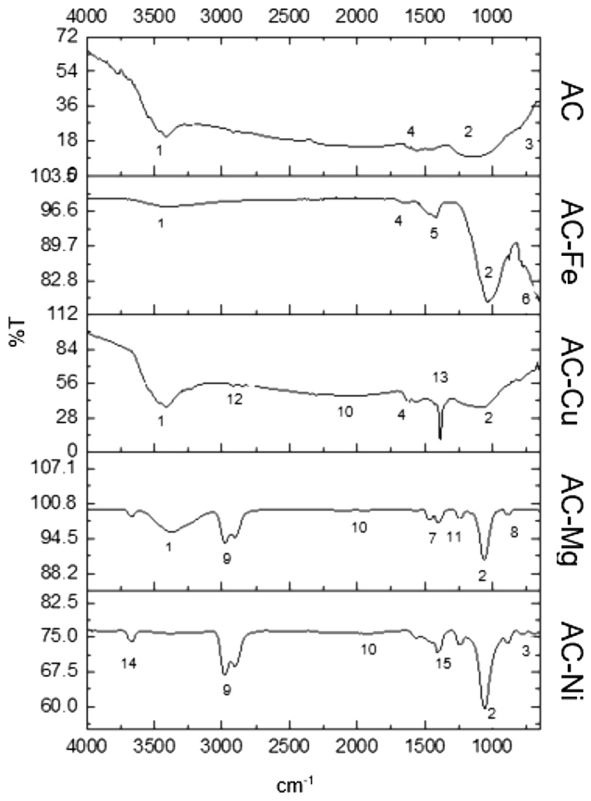

Fig. 5. FTIR spectra for pure and impregnated support with metals. ** caption□ 1: OH; 2: SiOH or C–O; 3: Si-O-Si; 4: C=C; 5: FeOOH; 6: Fe_2O_3; 7: $Mg-NO_2$; 8: MgO; 9: –CH; 10: $C=O/NH^+$; 11: $MgCO_3$; 12: Cu-N; 13: copper attached to the hydroxyl group; 14:oxidation state (+2) of impregnated Ni;15: region of the conjugation of the di-aryl group.

99].

For AC samples impregnated with nickel nitrate, a band at 3459 cm^{-1} can evidence the oxidation state (+2) of the impregnated nickel. Methylene ($–CH_2$) and the methyl ($–CH_3$) groups stretching bands appears at 2848–3032 cm^{-1}. Around 1450–1650 cm^{-1}, one can see the band referring to C=C, and at 670–900cm^{-1}, the –CH bond. Carbonyl and carboxyl group bands appear between 1860–1650 cm^{-1} [67,101].

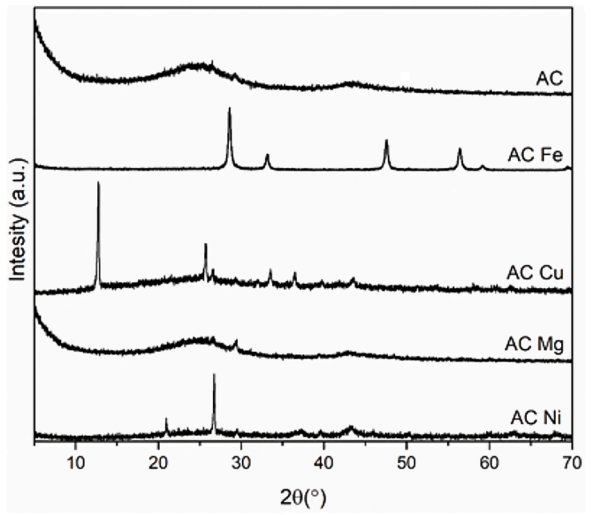

Fig. 6. XRD of activated carbon (AC) and AC impregnated with metals.

3.1.5. DRX

The XRD analysis samples of pure AC and AC impregnated with iron nitrate, copper nitrate, magnesium nitrate, and nickel nitrate is shown in Fig. 6.

The AC sample showed carbon and graphite carbon planes at an angle of 2Θ close to 25° and 43°. Diffraction peaks below 25° and close to 44° are probably related to the carbonic graphite hexagonal structure. The absence of diffraction peaks below 25° is most likely due to a disturbance of the graphitic carbon structure due to the iron interaction with carbon atoms [88].

For AC-Fe samples, the graphite structure formed by the catalytic action of iron particles (ion Fe^{3+}) impregnated in carbon appears at 26.2° [89]. Diffraction peaks around 59° and 62.5° correspond to (511) and (440) planes of Fe_3O_4 [88,90–93]. Besides, a peak near 25° corresponds to goethite (120) (JCPDS Card n°. 29-0713), at 35° and 45° to hematite (104) (JCPDS Card n°. 33-0664) or goethite (021), at 45° and 55° to hematite (024) and (116) [94]. According to Ramirez et al. [95], peaks at 26° and 43° are associated with AC typical turbostratic structure and, close to 35°, FeO (111) (JCPDS Card n°. 74-1886) phases may be present.

Copper impregnation caused interference in the structural plane due to copper in the form of copper oxide at 35.4° and 38.6°, which correspond to CuO (JCPDS Card n°. 48-1548) [96]. The small peak around 44.2° corresponds to the metallic copper plane (111) (JCPDS Card n°.4-836). Besides, the peak around 25.0° is attributed to the plane (002) of amorphous carbon [97].

The X-ray diffractogram of AC-Mg showed no significant difference to the pure support, presenting a broad peak between 20° and 30° attributed to activated carbon. The absence of peaks in the AC-Mg sample is attributed to the amorphous MgO structures formed in the activated carbon [98].

For the AC-Ni sample, peaks around 22° and 27° were attributed to carbon structures of activated carbon. The peak at 45° corresponds to the crystalline plane (200) of NiO (JCPDS Card n°. 04-0835) [100].

3.2. DMC synthesis reactions

3.2.1. DMC synthesis reactions using activated carbon impregnated with metals as catalysts

Table 2 presents methanol conversions, DMC yield, and selectivity values for reactions using the supported catalysts.

Surprisingly, bare AC is active in the DMC synthesis resulting in a yield of 5.5 % (Entry1, Table 2). The catalytic activity occurred most likely due to metals present in the pure coal structure, mainly iron, according to the ICP-OS analysis performed on the samples (Table S1). The AC-Fe sample obtained the highest yield, reaching 23.5 % with 100 % selectivity (Entry 2, Table 2). The AC-Cu also showed an acceptable

Table 2
Conversions, yields, and selectivity of reactions using catalysts supported on activated carbon. Reactions were performed using 213 mmol of methanol, 20 mmol of CH_3 I, 2.0 g of molecular sieves, 40 bar pressure, the temperature of 80 °C and the time of 24 h. The letters refer to the Tukey Test, where the same letters mean the statistical equality between the samples.

ENTRY	CATALYST	DMC SELECTIVITY (%)	METHANOL CONVERSION (%)	DMC YIELD (%)
1	AC	100	5.5 ± 0.6^c	5.5 ± 0.6^c
2	AC- Fe $(NO_3)_3$	100	23.5 ± 0.8^a	23.5 ± 0.8^a
3	AC-Cu $(NO_3)_2$	100	18.4 ± 0.9^b	18.4 ± 0.9^b
4	AC-Mg $(NO_3)_2$	100	4.0 ± 0.2^c	4.0 ± 0.2^c
5	AC-Ni $(NO_3)_2$	100	4.8 ± 0.6^c	4.8 ± 0.6^c
6	$Fe(NO_3)_3$	100	2.8 ± 0.6^d	2.8 ± 0.6^d
7	$Ni(NO_3)_2$	–	Traces	Traces

catalytic activity resulting in a DMC yield of 18.4 % and selectivity of 100 % (Entry 3, Table 2). AC -Mg (Entry 4, Table 2) and AC -Ni (Entry 5, Table 2) showed low catalytic activity resulting in 4.0 % and 4.8 % of DMC yields with 100 % selectivity. We also tested pure iron nitrate as a catalyst (see Entry 6, Table 2), resulting in low DMC yield (2.8 %) and 100 % of selectivity and $Ni(NO_3)_2$ (see Entry 7, Table 2), producing only DMC traces. As seen in Table 2, the selectivity was 100 % for all catalytic systems. Fig. S3 shows a typical chromatographic analysis for Ac-X samples exemplified when using Ac-Fe as catalyst (Table 2, entry 2), evidencing only the peaks belonging to methanol in 1.7 min, the solvent in 2.0, and DMC close to 2.6 min. These results corroborate that metal impregnation in AC improves the catalytic activity in DMC direct synthesis. Simulation results confirmed the need for the catalyst to foster the reaction (see Table 4), decreasing the reaction barrier due to the electrostatic interaction of the oxygen atom and the metal ion.

The letters above the results represent the Tukey Test to demonstrate statistical equality among the supported catalyst performance. As seen, AC, AC-Mg, and AC-Ni are statistically equal and, AC-Fe and AC-Cu are statistically different from the others. Therefore, among the evaluated, supported catalysts, AC–Fe proved to be the best. Thus, the catalytic performance follows the order: AC-Fe > AC-Cu > AC = AC-Mg = AC-Ni > $Fe(NO_3)_3$> $Ni(NO_3)_2$.

TGA findings showed that the iron nitrate impregnation on activated carbon was more satisfactory than Cu, Mg, and Ni (Fe = 18.38 %; Cu = 13.41 %; Mg = 8.17 %; Ni = 6.03 %). The higher catalytic performance is most likely related to the higher metal-impregnated content in the support, corroborated by simulation founds (see section 3.2.3). Yet, metal acidity is a determining factor for catalytic activity. Fe^{3+} presents a hard acid character reacting efficiently with a hard base (methanol) [102–104]. On the other hand, Cu^{2+}, Mg^{2+}, and Ni^{2+} have an intermediate acid character, making them less susceptible to react with a hard base (methanol) [102–104].

Table 1 shows no concrete relation between the specific surface area and the supported catalyst activity. Therefore, the impregnated support structure analysis may indicate that metals are present on the support surface and pores. However, it does not show direct influence on the catalytic action [38,39,63,67,75,105].

Li et al. [106] evaluated the combination of iron and zirconia, in different proportions, as a catalyst in the DMC direct synthesis (110 °C, 5 bar, and 4 h of reaction). They evidenced that the increase in the number of iron particles increases DMC yield. Therefore, the use of $Fe_{0.7}Zr_{0.3}O_y$ presented a DMC yield of 4 % and 100 % selectivity, concluding that the combination of zirconia with iron was fundamental to increase yield and selectivity. Chen et al. [38] evaluated the use of copper chloride impregnated in activated carbon in the DMC direct synthesis (25 °C and 140 bar), reaching around 5.0 % of methanol conversion and up to 90 % selectivity. Therefore, the combination of copper with the activated carbon structure influenced the increase in conversion and the product selectivity, obtaining a DMC yield of 4.5 %. Table 3 presents some literature related to DMC synthesis and different catalysts used to increase DMC yield.

We noticed that several studies refer to catalysts and dehydrating agents in the DMC direct synthesis (Table 3). The present work (Entry 1 and 2, Table 3) presents good DMC yield values compared to the literature. Each catalyst interacts differently in the reaction, so pressure and temperature parameters influence DMC yield and selectivity, as demonstrated by simulation results (see Section 3.2.3). Entry 1 and Entry 2 showed that a combination of the temperature of 80 °C and a pressure of 40 bar was efficient to promote an effective yield, however, we expect that changing these two parameters can lead to a considerable improvement in DMC yield.

Stoian et al. [110] used Mg-Al hydrotaleite on silica Lyogel at 130 °C and 10 bar, reaching a yield of approximately 16 %. On the other hand, Wang et al. [112] and Chen et al. [112] chose to insert dehydrating agents (DMP and molecular sieves), achieving low DMC yields (3.2 % and 5.0 %).

Thus, parameters such as pressure, temperature, time, catalyst amount, and the presence of dehydrating agents and promoters influence the catalytic activity of catalysts in the direct DMC synthesis.

Table 4
Gibbs free energies computed from electronic wave functions and vibrational frequencies for different reaction pathways at different conditions corresponding to the experimental setups in this research work. DMC and HI are produced out of CH_3OH, CH_3I, and CO_2. Thermochemistry for DMC and H_2O produced out of two methanol molecules and one carbon dioxide molecule (alternative transformation) was computed to show that this reaction is less energetically favorable at all physically sound conditions, as compared to the reaction involving the methyl iodide promoter: $CH_3OH + CH_3I + CO_2 = DMC + HI$. The precise procedure of thermochemistry calculation is described elsewhere [120].

Conditions		Gibbs free energy for different products, kJ mol^{-1}	
T, °C	P, bar	$CH_3OH + CH_3I + CO_2 = DMC + HI$	$2CH_3OH + CO_2 = DMC + H_2O$
25	1	46	69
25	50	36	60
80	50	43	67
130	50	49	74
80	1	54	79
80	40	44	68
80	100	41	65
80	200	39	63

3.2.2. Parameter optimization for direct DMC synthesis

As seen, AC-Fe is the most effective catalyst; however, factors such as catalyst amount, temperature, and pressure parameters can improve the reaction yield [6,8,10,12,42,85,113]. Fig. 7 shows the conversion and selectivity when using the AC-Fe catalyst in different quantities.

We noticed that the use of 0.4 g of AC-Fe showed a low methanol conversion (~4.0 %), whereas the increase of catalyst content to 0.55 g increased the conversion to ~16.0 %. When expanding to 0.7 g, a significant methanol conversion increase was observed, reaching 23.5 %. Also, a decrease in conversion was observed when increasing the AC-Fe catalyst content to 1.0 g and 1.3 g. The addition of a more significant amount of AC-Fe does not increase the methanol conversion. The selectivity was 100 % in both reactions. Al-Darwish et al. [114] observed the same behavior for cobalt oxide, showing that concentrations in the

Table 3
Available literature data in the area of DMC synthesis.

Entry	Catalyst	Promoter/ dehydrating agent	Temperature (°C)	Pressure (bar)	Yield (%)	Literature
1	AC-Fe	CH_3I/molecular sieves	80	40	23.5	This work
2	AC-Cu	CH_3I/molecular sieves	80	40	18.4	This work
3	Cu-Ni/graphene	–	110	30	13	Deerattraku et al. [107]
4	K_2CO_3	–	120	50	~3	Liu et al. [91]
5	$Fe_{0.7}Zr_{0.3}O_y$	–	110	50	~4.0	Li et al. [106]
6	$Ti_{0.04}Ce_{0.96}O_2$	–	120	80	~4.0	Fu et al. [108]
7	Cu–Ni/Zeolitic Imidazolate	–	110	20	~7.0	Poungsombate et al. [109]
8	Mg-Al Hydrotaleite/Silica Lyogel	–	130	10	~16.0	Stoian et al. [110]
9	CeO_2	DMP	140	50	3.2	Wang et al. [111]
8	Cu-Ni/molecular sieves	Molecular sieves 4A	120	110	5.0	Chen et al. [112]

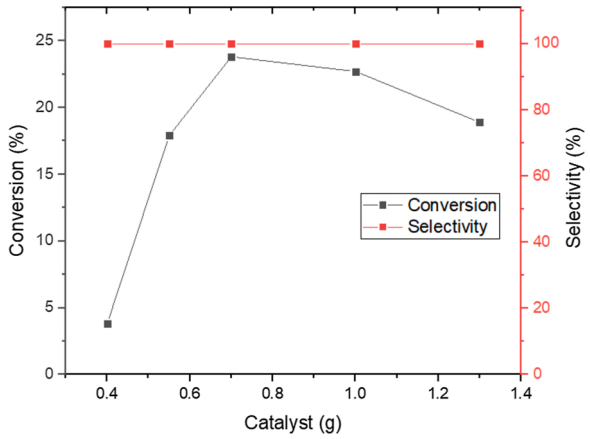

Fig. 7. Methanol conversion and selectivity using different amounts of the supported catalyst (AC-Fe). Reactions were performed using 213 mmol of methanol, 20 mmol of CH_3 I, 40 bar pressure, the temperature of 80 °C and the time of 24 h.

range of 2.5 %–10.0 % were efficient in the DMC synthesis; however, higher values decrease the DMC yield. Thus, with the use of 0.7 g of AC-Fe, the study of temperature and pressure parameters optimization was carried out. Fig. 8 presents the contour chart for DMC direct synthesis at different pressures and temperatures.

To achieve the highest DMC yield (above 25 %), a higher temperature (120 °C) and pressure around 40 bar will be needed, as seen in Fig. 8. The response surface graph (Fig. S4) proves that higher temperatures and medium pressures favor DMC yield when using AC-Fe as a catalyst (0.7 g) and 24 h of reaction time.

Xuan et al. [115] evaluated the use of MOF-808-X as a catalyst in DMC direct synthesis, concluding that increasing temperature up to 140 °C results in a DMC yield improvement. Also, they noticed that pressure and catalyst amount improved process efficiency to the point of stabilization. The yield curve of the synthesis remains constant. Chen et al. [116] analyzed the use of $Ti_xCe_{1-x}O_2$, concluding that at higher temperatures (120–140 °C) and mild pressures (12–24 bar), methanol conversion becomes more efficient, enabling to reach up to 24.3 % conversion, 70.5 % of selectivity, approximately 17 % of DMC yield (140 °C and 24 bar) and, 10.1 % conversion and 88 % selectivity, with about 8.8 % yield (100 °C and 12 bar). They also evidenced that oxygen species from adsorbed CO_2 can fill the catalyst surface vacancies playing a crucial role in promoting methanol and carbon dioxide catalytic conversion into DMC. Functional theory suggests that the cleavage of O=C=O bonds is energetically less endothermic when an oxygen atom

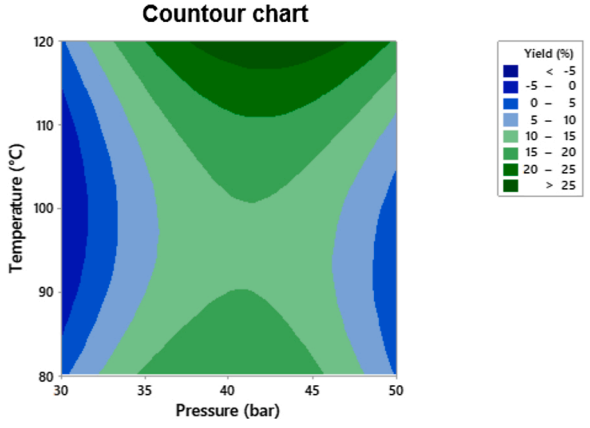

Fig. 8. Contour chart for DMC yield at different temperatures and pressures. Reactions were performed using 213 mmol of methanol, 20 mmol of CH_3I, 0.7 g of catalyst (AC-Fe), and 24 h time.

of CO_2 fills an empty oxygen site [116].

According to the DMC direct synthesis thermodynamics, the excessive temperature increase is unfavorable for the energetic process efficiency [117]. Studies indicate that the increase in yield for carbonate production occurs at a specific temperature. Pressure intervals need to be optimized and other reaction parameters such as catalyst, dehydrating agents, among others [118,119]. Therefore, for the use of AC-Fe as a catalyst in DMC direct synthesis, higher temperatures, and mild pressures are necessary to achieve higher conversion, selectivity, and, consequently, yield. In the tested system, the temperature of 120 °C using AC-Fe as a catalyst combined with the other reaction conditions (pressure = 40 bar, time = 24 h, catalyst = 0.7 g) is efficient for DMC direct synthesis. Stepwise simulations of the DMC formation reaction and the energy barrier detected (see Fig. 9 and Table 4) corroborated the need for elevated temperatures to produce DMC as a primary reaction product.

3.2.3. Simulation results

The major reaction steps are depicted in Fig. 9. We also exemplify simplified models of complexes involving metallic catalysts and reactants (carbon dioxide and methanol). The reaction starts with CO_2 attachment to CH_3OH (Fig. 9a) that is fostered by the catalyst. Transfer of the hydrogen atom becomes possible. Next, DMC and hydrogen iodide are formed (Fig. 9b). Thanks to possessing non-zero electric moments (dipole one in case of CH_3OH and quadruple one in case of CO_2), both reactants strongly interact with the catalyst particle, see Fig. 9c,d, that is adsorbed on AC.

The synthesis of DMC, despite a positive role of the metal ions, is energetically tough (Table 4). We provide thermochemistry calculations for DMC formation out of CH_3OH, CO_2, and CH_3I along with a simplified pathway that involves 2 methanol molecules and CO_2. Comparison of mechanisms involving $CH_3OH + CH_3I + CO_2 = DMC + HI$ and $2CH_3OH + CO_2 = DMC + H_2O$ clearly reveals that the former one is more thermodynamically favorable at all considered experimental conditions. Thus, the presence of CH_3I as a promoter in this work makes practical sense.

Analysis of the Gibbs free energies at different confirms the principal impossibility to achieve high yields of DMC using the proposed reaction schemes become the reaction Gibbs free energy is directly proportional to the reaction equilibrium constant. Pressure increase shifts equilibrium towards the products for both reactions, but the effect of a significant pressure increase is rather modest (Table 4). Elevated temperatures used in our experimental setups are unfavorable for the reaction Gibbs free energies and hence shifts equilibrium towards reactants. However, they were absolutely necessary to get an essential fraction of DMC as a major reaction product in the experimental studies. This observation allows us to hypothesize that the DMC formation reaction is associated with rather high energy barriers that are only partially decreased by the metallic catalysts adsorbed on AC.

3.2.4. Evaluation of the reuse of the AC-Fe catalyst

As discussed earlier, the AC-Fe catalyst at 120 °C of temperature and mild pressures (40 bar) were the reaction conditions optimized for DMC direct synthesis. AC-Fe catalyst recycling (4 cycles), using different dehydrating agent systems (sieve and DMF) separately and combined, and the optimized reaction conditions can be seen in Fig. 10.

We noticed that system A (molecular sieve in the gaseous phase) presented the highest methanol conversion since the initial recycling (recycle 0) reached approximately 30 % methanol conversion and 100 % selectivity. A methanol conversion decrease was observed in the first recycle (recycle 1 = approximately 22 %). However, a slight decrease was observed in the other cycles (recycle 2 = approximately 20 %; recycle 3 = approximately 19 % and recycle 4 = approximately 18 %). Selectivity in all recycles for system A remained 100 %; there was no by-products formation during the process in all recycles.

For the B system (DMP in the liquid phase), the initial methanol

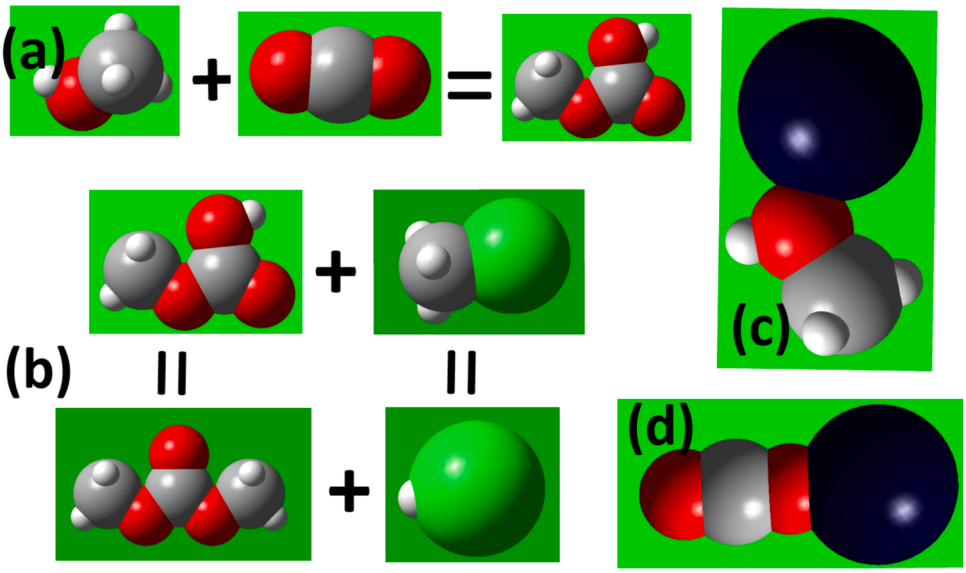

Fig. 9. Major intermediates detected during the formation of DMC out of methanol, carbon dioxide, and methyl iodide: (a) $CH_3OH + CO_2 = CH_3O\text{-}COO\text{-}H$; (b) $CH_3O\text{-}COO\text{-}H + CH_3I = CH_3\text{-}O\text{-}C(O)\text{-}O\text{-}CH_3 + HI$; (c) electrostatically bound complex of Fe^{3+} and CH_3OH; (d) electrostatically bound complex of Fe^{3+} and CO_2. The geometries of the depicted molecules and molecular complexes were optimized quantum chemically to minimize the potential energy of the system in each case. The resulting Z-matrices were subsequently used to calculate Gibbs free energies for the proposed reaction stages.

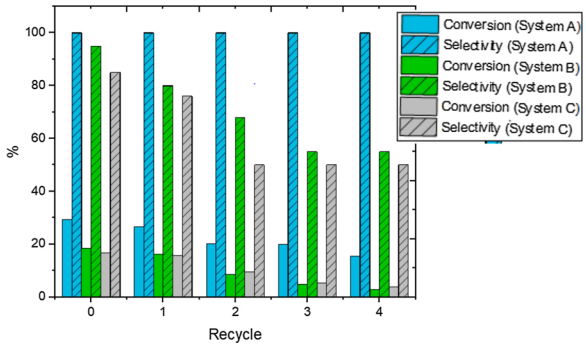

Fig. 10. The conversion and the selectivity of DMC synthesis using the AC-Fe catalyst. A: molecular sieve 4A (dehydrating agent); B: DMP (dehydrating agent); C: molecular sieve (gas phase) combined with DMP (liquid phase). * Pressure: 40 bar; Temperature: 120 °C; Time: 24 h; 0.7 g of AC-Fe; 2.0 g of molecular sieve; 10 mmol of DMP; 213 mmol methanol;20 mmol of CH_3I.

conversion (recycle 0) of approximately 18 % remained constant in the first recycle (recycle 1). However, we noticed a drastic methanol conversion decrease, down to 3 %, in the recycle 4. Also, DMP in the liquid phase produces a by-product (ketone), decreasing DMC yield and selectivity during the reuse needing a DMP purification step [4]. Therefore, the DMP in the liquid phase does not improve methanol conversion and selectivity when used for catalyst recycling. On the other hand, system C (sieve combined with DMP) showed similar methanol conversion and selectivity to system B throughout the recycles. Thus, the DMP present in the liquid phase may be preventing the action of molecular sieves in the gas phase and impairing the system's dehydration.

Several studies on catalyst recycling are described in the literature, aiming to reduce DMC production costs [114,117,121,122]. Al-Daewish et al. [114], analyzed CeO_2 as a catalyst in different forms for DMC synthesis, namely: CeO_2, CoO/ CeO_2, NiO/ CeO_2, CaO/ CeO_2 and CuO/ CeO_2. Reuse was evaluated under reaction conditions of 140 °C, 30 bar, 3 h, and 0.5 g catalyst. The maximum yield for CeO_2 was found to be at 1.6 mmol of DMC. Through the four recycles, the catalyst activity decreased each cycle. CaO/CeO_2 only feature activity for two cycles. CuO/CeO_2 was effective only in the first one showing that each catalyst interacts differently in the reaction medium, possibly reused or not in the DMC synthesis [114].

4. Conclusions

The characterization analysis of the catalysts (AC-Fe, AC-Cu, AC-Mg, and AC-Ni) showed that the activated carbon metal impregnation was successful, most likely due to numerous pores in its structure, and the best impregnation occurred for AC-Fe. The catalytic reactions stressed that the use of AC-Fe catalyst has proved to be the most efficient in the DMC direct synthesis than other metals, with a yield of 23.5 % and selectivity of 100 %. Simulation results evidenced the need for the metal catalyst to foster the reaction.

The process optimization indicated that in the amount of 0.7 g of the catalyst (AC-Fe), 40 bar of pressure, and 120 °C of temperature, the best conversion, selectivity, and, consequently, DMC yield (approximately 30 %) occurs. Stepwise simulations of the DMC formation reaction and the energy barrier explained the need for elevated temperatures in experimental setups to get an essential fraction of DMC as a primary reaction product.

The evaluation of catalytic systems A, B, and C proved that system A is the most suitable for catalyst reuse since it does not alter the product selectivity and does not abruptly decrease reaction yield.

CRediT authorship contribution statement

Douglas José Faria worked on conceptualization, investigation, Methodology, and writing. **Leonardo Moreira dos Santos** worked on conceptualization, investigation, Project administration, and writing. **Franciele L. Bernard** worked on conceptualization, investigation, Project administration. **Ingrid Selbacch Pinto** worked on investigation and validation. **Ivan Pacheco Romero** worked on resources and supervision. **Vitaly V Chaban** worked on Methodology, formal analysis, Investigation, validation and writing. **Sandra Einloft** worked on conceptualization, Methodology, Project administration, funding acquisition, and writing.

Declaration of Competing Interest

The authors declare that they have no known competing financial interests or personal relationships that could have appeared to influence the work reported in this paper.

Acknowledgments

Douglas Faria thanks CAPES; Sandra Einloft thanks CNPq for the

research scholarship. This study was financed in part by the Coordenação de Aperfeiçoamento de Pessoal de Nível Superior – Brasil (CAPES) – Finance Code 001. The authors thank Petrobras for financial support and the strategic importance of the support given by ANP (Brazil's National Oil, Natural Gas, and Biofuels Agency) through the R&D levy regulation.

Appendix A. Supplementary data

Supplementary data associated with this article can be found, in the online version, at https://doi.org/10.1016/j.jcou.2021.101721.

References

[1] I. Ganesh, Conversion of carbon dioxide into methanol – a potential liquid fuel: fundamental challenges and opportunities (a review), Renewable Sustainable Energy Rev. 31 (March) (2014) 221–257, https://doi.org/10.1016/j.rser.2013.11.045.

[2] N. Miralles, J.E. Gómez, A.W. Kleij, E. Fernández, Copper-mediated S N 2′ allyl–Alkyl and allyl–Boryl couplings of vinyl cyclic carbonates, Org. Lett. 19 (November 22) (2017) 6096–6099, https://doi.org/10.1021/acs.orglett.7b02947.

[3] Z. Xu, et al., Enhanced performance of a lithium-sulfur battery using a carbonate-based electrolyte, Angew. Chemie Int. Ed. 55 (August 35) (2016) 10372–10375, https://doi.org/10.1002/anie.201605931.

[4] D.J. Faria, L. Moreira dos Santos, F.L. Bernard, I. Selbacch Pinto, M.A. Carmona da Motta Resende, S. Einloft, Dehydrating agent effect on the synthesis of dimethyl carbonate (DMC) directly from methanol and carbon dioxide, RSC Adv. 10 (57) (2020) 34895–34902, https://doi.org/10.1039/D0RA06034H.

[5] T. Sakakura, J.-C. Choi, H. Yasuda, Transformation of carbon dioxide, Chem. Rev. 107 (June 6) (2007) 2365–2387, https://doi.org/10.1021/cr068357u.

[6] A.A. Marciniak, O.C. Alves, L.G. Appel, C.J.A. Mota, Synthesis of dimethyl carbonate from CO2 and methanol over CeO2: role of copper as dopant and the use of methyl trichloroacetate as dehydrating agent, J. Catal. 371 (March) (2019), https://doi.org/10.1016/j.jcat.2019.01.035.

[7] A.A. Marciniak, et al., What are the preferred CeO2 exposed planes for the synthesis of dimethyl carbonate? Answers from theory and experiments, Mol. Catal. 493 (September) (2020), https://doi.org/10.1016/j.mcat.2020.111053.

[8] A. Sánchez, L.M. Gil, M. Martín, Sustainable DMC production from CO2 and renewable ammonia and methanol, J. Co2 Util. 33 (October) (2019) 521–531, https://doi.org/10.1016/j.jcou.2019.08.010.

[9] A.A. Chaugule, A.H. Tamboli, H. Kim, Ionic liquid as a catalyst for utilization of carbon dioxide to production of linear and cyclic carbonate, Fuel, vol. 200 (July) (2017), https://doi.org/10.1016/j.fuel.2017.03.077.

[10] B.A.V. Santos, V.M.T.M. Silva, J.M. Loureiro, A.E. Rodrigues, Review for the direct synthesis of dimethyl carbonate, Chembioeng Rev. 1 (October 5) (2014), https://doi.org/10.1002/cben.201400020.

[11] G. Fiorani, A. Perosa, M. Selva, Dimethyl carbonate: a versatile reagent for a sustainable valorization of renewables, Green Chem. 20 (2) (2018), https://doi.org/10.1039/C7GC02118F.

[12] H.-Z. Tan, et al., Review on the synthesis of dimethyl carbonate, Catal. Today 316 (October) (2018), https://doi.org/10.1016/j.cattod.2018.02.021.

[13] S. Cui, J. Borgemenke, Z. Liu, H.M. Keener, Y. Li, Innovative sustainable conversion from CO2 and biodiesel-based crude glycerol waste to bio-based polycarbonates, J. Co2 Util. 34 (December) (2019) 198–206, https://doi.org/10.1016/j.jcou.2019.06.004.

[14] W. Deng, L. Shi, J. Yao, Z. Zhang, A review on transesterification of propylene carbonate and methanol for dimethyl carbonate synthesis, Carbon Resour. Convers. 2 (December 3) (2019), https://doi.org/10.1016/j.crcon.2019.10.004.

[15] A.H. Tamboli, A.A. Chaugule, S.W. Gosavi, H. Kim, Ce Zr1−O2 solid solutions for catalytic synthesis of dimethyl carbonate from CO2: reaction mechanism and the effect of catalyst morphology on catalytic activity, Fuel, vol. 216 (March) (2018), https://doi.org/10.1016/j.fuel.2017.12.008.

[16] A.H. Tamboli, A.A. Chaugule, H. Kim, Catalytic developments in the direct dimethyl carbonate synthesis from carbon dioxide and methanol, Chem. Eng. J. 323 (September) (2017), https://doi.org/10.1016/j.cej.2017.04.112.

[17] A.A. Greish, E.D. Finashina, O.P. Tkachenko, E.V. Shuvalova, L.M. Kustov, Synthesis of dimethyl carbonate from methanol and CO2 on the SnO2/Al2O3-based catalyst, Mendeleev Commun. 26 (November 6) (2016), https://doi.org/10.1016/j.mencom.2016.11.012.

[18] H. Zhao, B. Lu, X. Li, W. Zhang, J. Zhao, Q. Cai, Hydroxyl-functionalized ionic liquid for activation and conversion of CO2 and methanol into dimethyl carbonate, J. Co2 Util. 12 (December) (2015), https://doi.org/10.1016/j.jcou.2015.08.001.

[19] J. Du, J. Shi, Z. Li, Z. Liu, X. Fan, C. Tao, Ionic liquid mediated CO2 activation for DMC synthesis, J. Nat. Gas Chem. 21 (July 4) (2012), https://doi.org/10.1016/S1003-9953(11)60393-9.

[20] H.J. Lee, W. Joe, I.K. Song, Direct synthesis of dimethyl carbonate from methanol and carbon dioxide over transition metal oxide/Ce0.6Zr0.4O2 catalysts: effect of acidity and basicity of the catalysts, Korean J. Chem. Eng. 29 (March 3) (2012), https://doi.org/10.1007/s11814-011-0185-3.

[21] S.T. Hong, H.S. Park, J.S. Lim, Y.-W. Lee, M. Anpo, J.-D. Kim, Synthesis of dimethyl carbonate from methanol and supercritical carbon dioxide, Res. Chem. Intermed. 32 (August 8) (2006), https://doi.org/10.1163/156856706778606552.

[22] D. Ballivet-Tkatchenko, et al., Direct synthesis of dimethyl carbonate with supercritical carbon dioxide: characterization of a key organotin oxide intermediate, Catal. Today 115 (June 1–4) (2006), https://doi.org/10.1016/j.cattod.2006.02.025.

[23] Q. Cai, C. Jin, B. Lu, H. Tangbo, Y. Shan, Synthesis of dimethyl carbonate from methanol and carbon dioxide using potassium methoxide as catalyst under mild conditions, Catal. Letters 103 (October 3–4) (2005), https://doi.org/10.1007/s10562-005-7158-2.

[24] K. Tomishige, Y. Ikeda, T. Sakaihori, K. Fujimoto, Catalytic properties and structure of zirconia catalysts for direct synthesis of dimethyl carbonate from methanol and carbon dioxide, J. Catal. 192 (June 2) (2000), https://doi.org/10.1006/jcat.2000.2854.

[25] K. Tomishige, T. Sakaihori, Y. Ikeda, K. Fujimoto, A novel method of direct synthesis of dimethyl carbonate from methanol and carbon dioxide catalyzed by zirconia, Catal. Letters 58 (4) (1999), https://doi.org/10.1023/A:1019098405444.

[26] X. Jin, et al., Catalytic conversion of CO2 and shale gas-derived substrates into saturated carbonates and derivatives: catalyst design, performances and reaction mechanism, J. Co2 Util. 34 (December) (2019) 115–148, https://doi.org/10.1016/j.jcou.2019.05.024.

[27] W. Wang, Y. Zhang, Z. Wang, J. Yan, Q. Ge, C. Liu, Reverse water gas shift over in 2 O 3 –CeO 2 catalysts, Catal. Today 259 (January) (2016) 402–408, https://doi.org/10.1016/j.cattod.2015.04.032.

[28] B. Zhao, Y. Pan, C. Liu, The promotion effect of CeO2 on CO2 adsorption and hydrogenation over Ga2O3, Catal. Today 194 (October 1) (2012) 60–64, https://doi.org/10.1016/j.cattod.2012.05.011.

[29] J.F. Knifton, R.G. Duranleau, Ethylene glycol—dimethyl carbonate cogeneration, J. Mol. Catal. 67 (August 3) (1991) 389–399, https://doi.org/10.1016/0304-5102(91)80051-4.

[30] S. Fang, K. Fujimoto, Direct synthesis of dimethyl carbonate from carbon dioxide and methanol catalyzed by base, Appl. Catal. A Gen. 142 (August 1) (1996) L1–L3, https://doi.org/10.1016/0926-860X(96)00081-6.

[31] Z.-F. Zhang, Z.-T. Liu, Z.-W. Liu, J. Lu, DMC formation over Ce0.5Zr0.5O2 prepared by complex-decomposition method, Catal. Letters 129 (May 3–4) (2009) 428–436, https://doi.org/10.1007/s10562-008-9816-7.

[32] D. Stoian, F. Medina, A. Urakawa, Improving the Stability of CeO_2 Catalyst by Rare Earth Metal Promotion and Molecular Insights in the Dimethyl Carbonate Synthesis from CO_2 and Methanol with 2-Cyanopyridine, ACS Catal. 8 (April 4) (2018), https://doi.org/10.1021/acscatal.7b04198.

[33] P. Švec, R. Olejník, Z. Padělková, A. Růžička, L. Plasseraud, C,N-chelated organotin(IV) trifluoromethanesulfonates: synthesis, characterization and preliminary studies of its catalytic activity in the direct synthesis of dimethyl carbonate from methanol and CO2, J. Organomet. Chem. 708–709 (June) (2012) 82–87, https://doi.org/10.1016/j.jorganchem.2012.02.022.

[34] J. Kizlink, Synthesis of dimethyl carbonate from carbon dioxide and methanol in the presence of organotin compounds, Collect. Czech. Chem. Commun. 58 (6) (1993) 1399–1402, https://doi.org/10.1135/cccc19931399.

[35] S. Wada, K. Oka, K. Watanabe, Y. Izumi, Catalytic conversion of carbon dioxide into dimethyl carbonate using reduced copper-cerium oxide catalysts as low as 353 K and 1.3 MPa and the reaction mechanism, Front. Chem. 1 (2013), https://doi.org/10.3389/fchem.2013.00008.

[36] S. Akbayrak, Z. Özçifçi, A. Tabak, Noble metal nanoparticles supported on activated carbon: highly recyclable catalysts in hydrogen generation from the hydrolysis of ammonia borane, J. Colloid Interface Sci. 546 (June) (2019) 324–332, https://doi.org/10.1016/j.jcis.2019.03.070.

[37] N. Keller, G. Rebmann, V. Keller, Catalysts, mechanisms and industrial processes for the dimethylcarbonate synthesis, J. Mol. Catal. A Chem. 317 (February 1–2) (2010) 1–18, https://doi.org/10.1016/j.molcata.2009.10.027.

[38] J. Bian, X.W. Wei, Y.R. Jin, L. Wang, D.C. Luan, Z.P. Guan, Direct synthesis of dimethyl carbonate over activated carbon supported Cu-based catalysts, Chem. Eng. J. 165 (December 2) (2010) 686–692, https://doi.org/10.1016/j.cej.2010.10.002.

[39] P. Yang, Y. Cao, W.-L. Dai, J.-F. Deng, K.-N. Fan, Effect of chemical treatment of activated carbon as a support for promoted dimethyl carbonate synthesis by vapor phase oxidative carbonylation of methanol over Wacker-type catalysts, Appl. Catal. A Gen. 243 (April 2) (2003) 323–331, https://doi.org/10.1016/S0926-860X(02)00567-7.

[40] M.S. Han, B.G. Lee, I. Suh, H.S. Kim, B.S. Ahn, S.I. Hong, Synthesis of dimethyl carbonate by vapor phase oxidative carbonylation of methanol over Cu-based catalysts, J. Mol. Catal. A Chem. 170 (May 1–2) (2001) 225–234, https://doi.org/10.1016/S1381-1169(01)00073-5.

[41] Z. Li, K. Xie, R.C.T. Slade, High selective catalyst CuCl/MCM-41 for oxidative carbonylation of methanol to dimethyl carbonate, Appl. Catal. A Gen. 205 (January 1–2) (2001) 85–92, https://doi.org/10.1016/S0926-860X(00)00546-9.

[42] E. Leino, et al., Synthesis and characterization of ceria-supported catalysts for carbon dioxide transformation to diethyl carbonate, Catal. Today 306 (May) (2018) 128–137, https://doi.org/10.1016/j.cattod.2017.01.016.

[43] D.M. Rodrigues, et al., Imidazolium-based ionic liquid silica xerogel as catalyst to transform CO2 into cyclic carbonate, SN Appl. Sci. 2 (December 12) (2020) 1936, https://doi.org/10.1007/s42452-020-03712-z.

[44] M.W. Schmidt, et al., General atomic and molecular electronic structure system, J. Comput. Chem. 14 (November 11) (1993) 1347–1363, https://doi.org/10.1002/jcc.540141112.
[45] S.R. Bahn, K.W. Jacobsen, An object-oriented scripting interface to a legacy electronic structure code, Comput. Sci. Eng. 4 (3) (2002) 56–66, https://doi.org/10.1109/5992.998641.
[46] A.-R. Allouche, Gabedit-A graphical user interface for computational chemistry softwares, J. Comput. Chem. 32 (January 1) (2011) 174–182, https://doi.org/10.1002/jcc.21600.
[47] W. Humphrey, A. Dalke, K. Schulten, VMD: visual molecular dynamics, J. Mol. Graph. 14 (February 1) (1996) 33–38, https://doi.org/10.1016/0263-7855(96)00018-5.
[48] M.D. Hanwell, D.E. Curtis, D.C. Lonie, T. Vandermeersch, E. Zurek, G. R. Hutchison, Avogadro: an advanced semantic chemical editor, visualization, and analysis platform, J. Cheminform. 4 (December 1) (2012) 17, https://doi.org/10.1186/1758-2946-4-17.
[49] N.A. Andreeva, V.V. Chaban, Global minimum search via annealing: nanoscale gold clusters, Chem. Phys. Lett. 622 (February) (2015) 75–79, https://doi.org/10.1016/j.cplett.2015.01.026.
[50] V. Chaban, Competitive solvation of the imidazolium cation by water and methanol, Chem. Phys. Lett. 623 (March) (2015) 76–81, https://doi.org/10.1016/j.cplett.2015.01.051.
[51] V. Chaban, Hydrogen fluoride capture by imidazolium acetate ionic liquid, Chem. Phys. Lett. 625 (April) (2015) 110–115, https://doi.org/10.1016/j.cplett.2015.02.041.
[52] R. Peverati, D.G. Truhlar, Improving the accuracy of hybrid Meta-GGA density functionals by range separation, J. Phys. Chem. Lett. 2 (November 21) (2011) 2810–2817, https://doi.org/10.1021/jz201170d.
[53] S. Grimme, J. Antony, S. Ehrlich, H. Krieg, A consistent and accurate ab initio parametrization of density functional dispersion correction (DFT-D) for the 94 elements H-Pu, J. Chem. Phys. 132 (April 15) (2010) 154104, https://doi.org/10.1063/1.3382344.
[54] R.E. Easton, D.J. Giesen, A. Welch, C.J. Cramer, D.G. Truhlar, The MIDI! Basis set for quantum mechanical calculations of molecular geometries and partial charges, Theor. Chim. Acta 93 (May 5) (1996) 281–301, https://doi.org/10.1007/BF01127507.
[55] B. Qiao, T.-J. Wang, H. Gao, Y. Jin, High density silanization of nano-silica particles using γ-aminopropyltriethoxysilane (APTES), Appl. Surf. Sci. 351 (October) (2015) 646–654, https://doi.org/10.1016/j.apsusc.2015.05.174.
[56] P.K. Jal, M. Sudarshan, A. Saha, S. Patel, B.K. Mishra, Synthesis and characterization of nanosilica prepared by precipitation method, Colloids Surf. A Physicochem. Eng. Asp. 240 (June 1–3) (2004) 173–178, https://doi.org/10.1016/j.colsurfa.2004.03.021.
[57] P.D. Mines, et al., Granular activated carbon with grafted nanoporous polymer enhances nanoscale zero-valent iron impregnation and water contaminant removal, Chem. Eng. J. 339 (May) (2018) 22–31, https://doi.org/10.1016/j.cej.2018.01.102.
[58] V.L.I. Bentes, F.X. Nobre, I.C.L. Barros, P.R.C. Couceiro, Composite of iron phosphate-supported carbon from the açaí (Euterpe oleracea) as a solid catalyst for photo-Fenton reactions, Environ. Nanotechnol. Monit. Manag. 16 (December) (2021), https://doi.org/10.1016/j.enmm.2021.100520.
[59] J.D. Figueroa, T. Fout, S. Plasynski, H. McIlvried, R.D. Srivastava, Advances in CO2 capture technology—the U.S. Department of energy's carbon sequestration program, Int. J. Greenh. Gas Control. 2 (January 1) (2008), https://doi.org/10.1016/S1750-5836(07)00094-1.
[60] K. Vinayakumar, A. Palliyarayil, P. Seethur Prakash, S. Nandakumar, N. Shunmuga Kumar, S. Sil, Studies on the deactivation and activation of palladium impregnated carbon catalyst for environmental applications, Mater. Today Proc. 31 (2020) 631–639, https://doi.org/10.1016/j.matpr.2020.05.110.
[61] R. Zakaria, N.A. Jamalluddin, M.Z. Abu Bakar, Effect of impregnation ratio and activation temperature on the yield and adsorption performance of mangrove based activated carbon for methylene blue removal, Results Mater. 10 (June) (2021), https://doi.org/10.1016/j.rinma.2021.100183.
[62] P.D. Mines, et al., Granular activated carbon with grafted nanoporous polymer enhances nanoscale zero-valent iron impregnation and water contaminant removal, Chem. Eng. J. 339 (May) (2018), https://doi.org/10.1016/j.cej.2018.01.102.
[63] A. Mullick, S. Neogi, Ultrasound assisted synthesis of Mg-Mn-Zr impregnated activated carbon for effective fluoride adsorption from water, Ultrason. Sonochem. 50 (January) (2019) 126–137, https://doi.org/10.1016/j.ultsonch.2018.09.010.
[64] I. Justo-Reinoso, M.T. Hernandez, C. Lucero, W.V. Srubar, Dispersion and effects of metal impregnated granular activated carbon particles on the hydration of antimicrobial mortars, Cem. Concr. Compos. 110 (July) (2020) 103588, https://doi.org/10.1016/j.cemconcomp.2020.103588.
[65] J. Aravind Kumar, et al., One pot Green Synthesis of Nano magnesium oxide-carbon composite: preparation, characterization and application towards anthracene adsorption, J. Clean. Prod. 237 (November) (2019) 117691, https://doi.org/10.1016/j.jclepro.2019.117691.
[66] E.M. Kalhori, T.J. Al-Musawi, E. Ghahramani, H. Kazemian, M. Zarrabi, Enhancement of the adsorption capacity of the light-weight expanded clay aggregate surface for the metronidazole antibiotic by coating with MgO nanoparticles: studies on the kinetic, isotherm, and effects of environmental parameters, Chemosphere 175 (May) (2017) 8–20, https://doi.org/10.1016/j.chemosphere.2017.02.043.
[67] B.Y. Jibril, A.Y. Atta, Activated carbon incorporated with first-row transition metals as catalysts in hydrogen production from propane, Int. J. Hydrogen Energy 36 (May 10) (2011) 5951–5959, https://doi.org/10.1016/j.ijhydene.2011.01.115.
[68] S.S. Kiani, et al., Synthesis and adsorption behavior of activated carbon impregnated with ASZM-TEDA for purification of contaminated air, Diam. Relat. Mater. 108 (October) (2020) 107916, https://doi.org/10.1016/j.diamond.2020.107916.
[69] R. Shi, et al., Graphene supported Cu nanoparticles as catalysts for the synthesis of dimethyl carbonate: effect of carbon black intercalation, Mol. Catal. 445 (February) (2018), https://doi.org/10.1016/j.mcat.2017.12.002.
[70] Z. Teng, K. Han, J. Li, Y. Gao, M. Li, T. Ji, Ultrasonic-assisted preparation and characterization of hierarchical porous carbon derived from garlic peel for high-performance supercapacitors, Ultrason. Sonochem. 60 (January) (2020), https://doi.org/10.1016/j.ultsonch.2019.104756.
[71] Y. Juan, Q. Ke-qiang, Preparation of activated carbon by chemical activation under vacuum, Environ. Sci. Technol. 43 (May 9) (2009), https://doi.org/10.1021/es8036115.
[72] Y. Gao, Q. Yue, B. Gao, A. Li, Insight into activated carbon from different kinds of chemical activating agents: a review, Sci. Total Environ. 746 (December) (2020) 141094, https://doi.org/10.1016/j.scitotenv.2020.141094.
[73] S.S. Kiani, et al., Synthesis and adsorption behavior of activated carbon impregnated with ASZM-TEDA for purification of contaminated air, Diam. Relat. Mater. 108 (October) (2020), https://doi.org/10.1016/j.diamond.2020.107916.
[74] Z. Rao, et al., Efficient peroxydisulfate activation with nZVI/CuO@BC nanocomposite derived from wastes for degradation of tetrabromobisphenol A in alkaline environment, J. Hazard. Mater. 417 (September) (2021), https://doi.org/10.1016/j.jhazmat.2021.126029.
[75] T. Tsoncheva, et al., Cobalt- and iron-based nanoparticles hosted in SBA-15 mesoporous silica and activated carbon from biomass: effect of modification procedure, Solid State Sci. 48 (October) (2015) 286–293, https://doi.org/10.1016/j.solidstatesciences.2015.09.001.
[76] C.G. Okoye-Chine, C.O.L. Mbuya, T.S. Ntelane, M. Moyo, D. Hildebrandt, The effect of silanol groups on the metal-support interactions in silica-supported cobalt Fischer-Tropsch catalysts. A temperature programmed surface reaction, J. Catal. 381 (January) (2020) 121–129, https://doi.org/10.1016/j.jcat.2019.10.036.
[77] T.S. Anirudhan, T.A. Rauf, S.R. Rejeena, Removal and recovery of phosphate ions from aqueous solutions by amine functionalized epichlorohydrin-grafted cellulose, Desalination 285 (January) (2012) 277–284, https://doi.org/10.1016/j.desal.2011.10.014.
[78] J. Xu, et al., Different iron salt impregnated granular activated carbon (Fe-GAC) for perchlorate removal: characterization, performance and mechanism, Colloids Surf. A Physicochem. Eng. Asp. 509 (November) (2016) 99–108, https://doi.org/10.1016/j.colsurfa.2016.08.039.
[79] I. Shah, R. Adnan, W.S. Wan Ngah, N. Mohamed, Iron impregnated carbon materials with improved physicochemical characteristics, Mater. Sci. Eng. B 201 (November) (2015) 1–12, https://doi.org/10.1016/j.mseb.2015.07.004.
[80] O.M. Mailoud, A.H. Elsayed, A.H. Abo-Elazm, H.A. Fetouh, Synthesis and study the structure, optical, thermal and dielectric properties of promising Glycine copper Nitrate (GCN) single crystals, Results Phys. 10 (September) (2018) 512–520, https://doi.org/10.1016/j.rinp.2018.05.042.
[81] M.H. Habibi, Z. Rezvani, Nanostructure copper oxocobaltate fabricated by co-precipitation route using copper and cobalt nitrate as precursors: characterization by combined diffuse reflectance and FT infrared spectra, Spectrochim. Acta A. Mol. Biomol. Spectrosc. 130 (September) (2014) 309–312, https://doi.org/10.1016/j.saa.2014.04.057.
[82] I.H. Chowdhury, A.H. Chowdhury, P. Bose, S. Mandal, M.K. Naskar, Effect of anion type on the synthesis of mesoporous nanostructured MgO, and its excellent adsorption capacity for the removal of toxic heavy metal ions from water, RSC Adv. 6 (8) (2016) 6038–6047, https://doi.org/10.1039/C5RA16837F.
[83] J. Madarász, P.P. Varga, G. Pokol, Evolved gas analyses (TG/DTA–MS and TG–FTIR) on dehydration and pyrolysis of magnesium nitrate hexahydrate in air and nitrogen, J. Anal. Appl. Pyrolysis 79 (May 1–2) (2007) 475–478, https://doi.org/10.1016/j.jaap.2006.12.024.
[84] S. Xie, X. Han, Q. Kuang, Y. Zhao, Z. Xie, L. Zheng, Intense and wavelength-tunable photoluminescence from surface functionalized MgO nanocrystal clusters, J. Mater. Chem. 21 (20) (2011) 7263, https://doi.org/10.1039/c1jm10745c.
[85] K. Zhang, et al., Wide pH range for fluoride removal from water by MHS-MgO/MgCO3 adsorbent: kinetic, thermodynamic and mechanism studies, J. Colloid Interface Sci. 446 (May) (2015) 194–202, https://doi.org/10.1016/j.jcis.2015.01.049.
[86] R. Haul, S. J. Gregg, K. S. W. Sing: Adsorption, Surface Area and Porosity. 2. Auflage, Academic Press, London 1982. 303 Seiten, Preis: $ 49.50, Berichte der Bunsengesellschaft für physikalische Chemie 86 (October 10) (1982), https://doi.org/10.1002/bbpc.19820861019, 957–957.
[87] X. Hu, H. Zhang, Z. Sun, Adsorption of low concentration ceftazidime from aqueous solutions using impregnated activated carbon promoted by Iron, copper and Aluminum, Appl. Surf. Sci. 392 (January) (2017) 332–341, https://doi.org/10.1016/j.apsusc.2016.09.047.
[88] S. Jain, et al., Enhancing adsorption of nitrate using metal impregnated alumina, J. Environ. Chem. Eng. 3 (December 4) (2015) 2342–2349, https://doi.org/10.1016/j.jece.2015.08.009.

[89] H.-H. Tseng, M.-Y. Wey, C.-H. Fu, Carbon materials as catalyst supports for SO2 oxidation: catalytic activity of CuO–AC, Carbon 41 (January 1) (2003) 139–149, https://doi.org/10.1016/S0008-6223(02)00264-6.
[90] C. Gai, F. Zhang, Q. Lang, T. Liu, N. Peng, Z. Liu, Facile one-pot synthesis of iron nanoparticles immobilized into the porous hydrochar for catalytic decomposition of phenol, Appl. Catal. B 204 (May) (2017) 566–576, https://doi.org/10.1016/j.apcatb.2016.12.005.
[91] Y. Wen, et al., Direct synthesis of dimethyl carbonate and propylene glycol using potassium bicarbonate as catalyst in supercritical CO2, Polish J. Chem. Technol. 17 (March 1) (2015) 62–65, https://doi.org/10.1515/pjct-2015-0010.
[92] Y. Tu, S. Tian, L. Kong, Y. Xiong, Co-catalytic effect of sewage sludge-derived char as the support of Fenton-like catalyst, Chem. Eng. J. 185–186 (March) (2012) 44–51, https://doi.org/10.1016/j.cej.2012.01.008.
[93] F. Duarte, F.J. Maldonado-Hódar, A.F. Pérez-Cadenas, L.M. Madeira, Fenton-like degradation of azo-dye Orange II catalyzed by transition metals on carbon aerogels, Appl. Catal. B 85 (January 3–4) (2009) 139–147, https://doi.org/10.1016/j.apcatb.2008.07.006.
[94] P. Mani, Y. Kim, S.K. Lakhera, B. Neppolian, H. Choi, Complete arsenite removal from groundwater by UV activated potassium persulfate and iron oxide impregnated granular activated carbon, Chemosphere 277 (August) (2021), https://doi.org/10.1016/j.chemosphere.2021.130225.
[95] J.H. Ramirez, F.J. Maldonado-Hódar, A.F. Pérez-Cadenas, C. Moreno-Castilla, C. A. Costa, L.M. Madeira, Azo-dye Orange II degradation by heterogeneous Fenton-like reaction using carbon-Fe catalysts, Appl. Catal. B 75 (September 3–4) (2007) 312–323, https://doi.org/10.1016/j.apcatb.2007.05.003.
[96] L. Bai, et al., Synthesis of a novel silica-supported dithiocarbamate adsorbent and its properties for the removal of heavy metal ions, J. Hazard. Mater. 195 (November) (2011) 261–275, https://doi.org/10.1016/j.jhazmat.2011.08.038.
[97] H. Li, et al., Remarkable activity of nitrogen-doped hollow carbon spheres encapsulated Cu on synthesis of dimethyl carbonate: role of effective nitrogen, Appl. Surf. Sci. 436 (April) (2018) 803–813, https://doi.org/10.1016/j.apsusc.2017.12.092.
[98] I.W. Siriwardane, et al., Synthesis and characterization of nano magnesium oxide impregnated granular activated carbon composite for H2S removal applications, Mater. Des. 136 (December) (2017), https://doi.org/10.1016/j.matdes.2017.09.034.
[99] I.W. Siriwardane, et al., Synthesis and characterization of nano magnesium oxide impregnated granular activated carbon composite for H2S removal applications, Mater. Des. 136 (December) (2017) 127–136, https://doi.org/10.1016/j.matdes.2017.09.034.
[100] M. Romero-Sáez, A.B. Dongil, N. Benito, R. Espinoza-González, N. Escalona, F. Gracia, CO2 methanation over nickel-ZrO2 catalyst supported on carbon nanotubes: a comparison between two impregnation strategies, Appl. Catal. B 237 (December) (2018), https://doi.org/10.1016/j.apcatb.2018.06.045.
[101] L.F. Sosa, V.T. da Silva, P.M. de Souza, Hydrogenation of levulinic acid to γ-valerolactone using carbon nanotubes supported nickel catalysts, Catal. Today (August) (2020), https://doi.org/10.1016/j.cattod.2020.08.022.
[102] N.R. Chereddy, K. Suman, P.S. Korrapati, S. Thennarasu, A.B. Mandal, Design and synthesis of rhodamine based chemosensors for the detection of Fe3+ ions, Dye. Pigment. 95 (December 3) (2012) 606–613, https://doi.org/10.1016/j.dyepig.2012.05.025.
[103] X. Wang, T. Li, A novel 'off-on' rhodamine-based colorimetric and fluorescent chemosensor based on hydrolysis driven by aqueous medium for the detection of Fe3+, Spectrochim. Acta A. Mol. Biomol. Spectrosc. 229 (March) (2020) 117951, https://doi.org/10.1016/j.saa.2019.117951.
[104] R.G. Pearson, Hard and soft acids and bases—the evolution of a chemical concept, Coord. Chem. Rev. 100 (April) (1990) 403–425, https://doi.org/10.1016/0010-8545(90)85016-L.
[105] E. Blanco, C. Sepulveda, K. Cruces, J.L. García-Fierro, I.T. Ghampson, N. Escalona, Conversion of guaiacol over metal carbides supported on activated carbon catalysts, Catal. Today 356 (October) (2020) 376–383, https://doi.org/10.1016/j.cattod.2019.08.029.
[106] A. Li, Y. Pu, F. Li, J. Luo, N. Zhao, F. Xiao, Synthesis of dimethyl carbonate from methanol and CO 2 over Fe–Zr mixed oxides, J. Co2 Util. 19 (May) (2017) 33–39, https://doi.org/10.1016/j.jcou.2017.02.016.
[107] V. Deerattrakul, A. Panitprasert, P. Puengampholsrisook, P. Kongkachuichay, Enhancing the dispersion of Cu-Ni metals on the graphene aerogel support for use as a catalyst in the direct synthesis of dimethyl carbonate from Carbon Dioxide and methanol, ACS Omega 5 (June 21) (2020) 12391–12397, https://doi.org/10.1021/acsomega.0c01143.
[108] Z. Fu, et al., TiO 2 -Doped CeO 2 nanorod catalyst for direct conversion of CO 2 and CH 3 OH to dimethyl carbonate: catalytic performance and kinetic study, ACS Omega 3 (January 1) (2018) 198–207, https://doi.org/10.1021/acsomega.7b01475.
[109] A. Poungsombate, T. Imyen, P. Dittanet, B. Embley, P. Kongkachuichay, Direct synthesis of dimethyl carbonate from CO 2 and methanol by supported bimetallic Cu–Ni/ZIF-8 MOF catalysts, J. Taiwan Inst. Chem. Eng. 80 (November) (2017) 16–24, https://doi.org/10.1016/j.jtice.2017.07.019.
[110] D.C. Stoian, E. Taboada, J. Llorca, E. Molins, F. Medina, A.M. Segarra, Boosted CO2 reaction with methanol to yield dimethyl carbonate over Mg–Al hydrotalcite-silica lyogels, Chem. Commun. 49 (48) (2013) 5489, https://doi.org/10.1039/c3cc41298a.
[111] S. Wang, J. Zhou, S. Zhao, Y. Zhao, X. Ma, Enhancement of dimethyl carbonate synthesis with in situ hydrolysis of 2,2-Dimethoxy propane, Chem. Eng. Technol. 39 (April 4) (2016) 723–729, https://doi.org/10.1002/ceat.201400603.
[112] H. Chen, S. Wang, M. Xiao, D. Han, Y. Lu, Y. Meng, Direct Synthesis of Dimethyl Carbonate from CO2 and CH3OH Using 0.4 nm Molecular Sieve Supported Cu-Ni Bimetal Catalyst, Chin. J. Chem. Eng. 20 (October 5) (2012) 906–913, https://doi.org/10.1016/S1004-9541(12)60417-0.
[113] M. Zhang, M. Xiao, S. Wang, D. Han, Y. Lu, Y. Meng, Cerium oxide-based catalysts made by template-precipitation for the dimethyl carbonate synthesis from Carbon dioxide and methanol, J. Clean. Prod. 103 (September) (2015), https://doi.org/10.1016/j.jclepro.2014.09.024.
[114] J. Al-Darwish, M. Senter, S. Lawson, F. Rezaei, A.A. Rownaghi, Ceria nanostructured catalysts for conversion of methanol and carbon dioxide to dimethyl carbonate, Catal. Today 350 (June) (2020) 120–126, https://doi.org/10.1016/j.cattod.2019.06.013.
[115] K. Xuan, Y. Pu, F. Li, J. Luo, N. Zhao, F. Xiao, Metal-organic frameworks MOF-808-X as highly efficient catalysts for direct synthesis of dimethyl carbonate from CO2 and methanol, Chinese J. Catal. 40 (April 4) (2019) 553–566, https://doi.org/10.1016/S1872-2067(19)63291-2.
[116] Y. Chen, et al., Ti x Ce 1−x O 2 nanocomposites: a monolithic catalyst for the direct conversion of carbon dioxide and methanol to dimethyl carbonate, Green Chem. 21 (17) (2019) 4642–4649, https://doi.org/10.1039/C9GC00811J.
[117] M. Zhang, et al., Catalytic materials for direct synthesis of dimethyl carbonate (DMC) from CO2, J. Clean. Prod. 279 (January) (2021) 123344, https://doi.org/10.1016/j.jclepro.2020.123344.
[118] H. Sun, et al., Nitrogen-doped carbon supported ZnO as highly stable heterogeneous catalysts for transesterification synthesis of ethyl methyl carbonate, J. Colloid Interface Sci. 581 (January) (2021) 126–134, https://doi.org/10.1016/j.jcis.2020.07.095.
[119] P. Kumar, L. Matoh, R. Kaur, U.L. Štangar, Synergic effect of manganese oxide on ceria based catalyst for direct conversion of CO2 to green fuel additive: catalyst activity and thermodynamics study, Fuel 285 (February) (2021) 119083, https://doi.org/10.1016/j.fuel.2020.119083.
[120] C.J. Cramer, Essentials of Computational Chemistry, second edition, Wiley, 2004.
[121] D. Dhana Lakshmi, B. Srinivasa Rao, N. Lingaiah, Synthesis of dimethyl carbonate from methanol and urea over zinc-strontia mixed oxide catalysts, Catal. Commun. 122 (March) (2019) 1–4, https://doi.org/10.1016/j.catcom.2019.01.005.
[122] J. Sun, B. Lu, X. Wang, X. Li, J. Zhao, Q. Cai, A functionalized basic ionic liquid for synthesis of dimethyl carbonate from methanol and CO2, Fuel Process. Technol. 115 (November) (2013), https://doi.org/10.1016/j.fuproc.2013.06.009.